INSTITUTE OF PHYSICS PUBLISHING JOURNAL OF MICROMECHANICS AND MICROENGINEERING

J. Micromech. Microeng. **16** (2006) 890–899 doi:10.1088/0960-1317/16/5/003

The nonlinear response of resonant microbeam systems with purely-parametric electrostatic actuation

Jeffrey F Rhoads[1], **Steven W Shaw**[1] **and Kimberly L Turner**[2]

[1] Department of Mechanical Engineering, Michigan State University, East Lansing, MI 48824, USA
[2] Department of Mechanical and Environmental Engineering, University of California—Santa Barbara, Santa Barbara, CA 93106, USA

E-mail: rhoadsje@msu.edu

Received 12 October 2005, in final form 27 January 2006
Published 24 March 2006
Online at stacks.iop.org/JMM/16/890

Abstract
Electrostatically-actuated resonant microbeam devices have garnered significant attention due to their geometric simplicity and broad applicability. Recently, some of this focus has turned to comb-driven microresonators with purely-parametric excitation, as such systems not only exhibit the inherent benefits of MEMS devices, but also a general improvement in sensitivity, stopband attenuation and noise rejection. This work attempts to combine each of these areas by proposing a microbeam device which couples the inherent benefits of a resonator with purely-parametric excitation with the simple geometry of a microbeam. Theoretical analysis reveals that the proposed device exhibits desirable response characteristics, but also quite complex dynamics. Of particular note is the fact that the device's nonlinear frequency response is found to be qualitatively dependent on the system's ac excitation amplitude. While this flexibility can be desirable in certain contexts, it introduces additional design and operating limitations. While the principal focus of this work is the proposed system's nonlinear response, the work also contains details pertaining to model development and device design.

1. Introduction

With reported successes in applications ranging from signal filtering to chemical and mass sensing, electrostatically-actuated resonant microbeam devices continue to be one of the most widely studied topics of the MEMS community. The devices' appeal can be traced to the fact that in addition to their inherent flexibility, they consume minimal power, are comparatively small, and are easy to fabricate due to their simple geometry (see, for example, [1–3]). Though electrostatically-actuated resonant microbeam systems, and most resonant MEMS devices in general, have traditionally been based on the usual linear resonance [2], a number of recent studies have indicated that the resonant behavior of such devices is often dependent on their nonlinear characteristics [1, 4–9]. Amongst the more interesting nonlinear effects are those generated by the electrostatic forces, which due to their position-dependent nature generally lead to some combination of direct and/or parametric excitation [1, 8]. Unfortunately, for typical microbeam designs such excitations occur in both a direct and parametric manner, thus yielding a predictable response, but eliminating (or reducing) the inherent benefits of designs based on purely-parametric excitations. In particular, known benefits such as nearly ideal stopband attenuation, comparatively higher sensitivity and high noise robustness are believed to be deteriorated (see, for example, [10, 11]). This work investigates a modified microbeam resonator design that is intended to recover the aforementioned benefits through a novel electrode configuration. In particular, it is shown that through the use of symmetric electrostatic actuation (as realized through exploitation of a three-plate capacitor design) direct excitation (and certain parametric excitation) effects which may hinder device performance can be eliminated or at least reduced to largely insignificant levels.

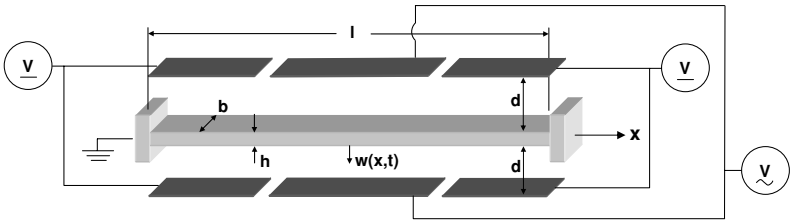

Figure 1. A schematic of a special case of the proposed microbeam system. Note that in this special case the beam is actuated by three electrode pairs, two of which provide dc excitation while the third provides ac excitation.

The general goal of this paper is to provide a brief, yet thorough, analysis of the proposed microbeam system, in particular, focusing on the local nonlinear response characteristics of such systems while paying attention to practical design issues, which may be beneficial for future experimental studies. Accordingly, the paper begins in section 2 with the presentation a continuous system model for a microbeam acted on by symmetric electrostatic actuation. Section 3 includes the formulation of a lumped-mass model for the system, which is better suited for systematic analysis. In section 4, the pull-in behavior of the system is briefly considered. Section 5, the principle focus of this work, explores the near-resonant response of the lumped-mass model and section 6 briefly discusses a variety of issues related to the design of practical devices based on the proposed system. The paper concludes in section 7 with some concluding remarks and an outline of future research and planned experimentation.

2. A continuous system model for a single microbeam

As a means of developing the lumped-mass model that forms the analytical basis for this work, a continuous system model is first considered. While a variety of such models have been proposed, that presented in [4, 8, 9], based on previous aeroelastic plate models presented in [12] and [13], is used as a starting point here.

Noting that a capacitively-actuated microbeam (the work can easily be extended to higher aspect ratio plate structures) is a suspended elastic beam with an applied electrostatic force (see figure 1), the equation of motion governing the transverse displacement of the beam, $w(x,t)$, is written as [4, 8, 9]

$$EI\frac{\partial^4 w}{\partial x^4}+\rho A\frac{\partial^2 w}{\partial t^2}+c\frac{\partial w}{\partial t}-\left[N+\frac{EA}{2l}\int_0^l\left(\frac{\partial w}{\partial x}\right)^2 \mathrm{d}x\right]\frac{\partial^2 w}{\partial x^2} = f_{es}(x,t), \tag{1}$$

where E and ρ (the modulus of elasticity and density, respectively) define the elastic material's properties, I defines the second moment of area, c delineates the viscous damping coefficient, N delineates a uniform applied axial force (a byproduct of typical microfabrication techniques) and $f_{es}(x,t)$ represents the electrostatic actuation force per unit length. As fixed–fixed microbeams are of primary interest here (the work is easily extendable to cantilevered beams), the system's boundary conditions, are given by

$$w(0,t)=0, \qquad w(l,t)=0,$$
$$\left.\frac{\partial w}{\partial x}\right|_{(0,t)}=0, \qquad \left.\frac{\partial w}{\partial x}\right|_{(l,t)}=0. \tag{2}$$

The electrostatic interaction between the beam and the multiple electrodes (see figure 1) is modeled as a parallel-plate capacitor with a single moving plate and minimal fringe field effects. Accordingly, the attractive electrostatic actuation force per unit length, $f_{es}(x,t)$, is written as

$$f_{es}(x,t)=\sum_i^P \frac{1}{2}\varepsilon_0 b\left[\frac{V_i^2(t)}{(d-w)^2}-\frac{V_i^2(t)}{(d+w)^2}\right] \times [H(x-a_i)-H(x-b_i)], \tag{3}$$

where

$$H(x-\varphi)=\begin{cases}1 & x\geqslant\varphi\\ 0 & x<\varphi\end{cases}, \tag{4}$$

ε_0 is the free space permittivity, and $V_i(t)$ is the actuation voltage applied to the ith electrode.

To facilitate analysis this equation is nondimensionalized in a manner similar to that presented in [4, 8, 9]. In particular, both the transverse displacement, w, and the spatial coordinate, x, are normalized by characteristic lengths of the system, the gap width and beam length, respectively, according to

$$\hat{w}=\frac{w}{d} \tag{5}$$

and

$$\hat{x}=\frac{x}{l}, \tag{6}$$

time is nondimensionalized by a characteristic period of the system according to

$$\hat{t}=\frac{t}{T}, \tag{7}$$

where

$$T=\sqrt{\frac{\rho bhl^4}{EI}}=\sqrt{\frac{12\rho l^4}{Eh^2}}, \tag{8}$$

and the input voltages are normalized by a characteristic voltage of the system, V_C (for example, the dc static pull-in voltage), according to

$$\hat{V}_i(\hat{t})=\frac{V_i(\hat{t})}{V_C}. \tag{9}$$

This procedure results in a system governed by the equation of motion

$$\frac{\partial^4\hat{w}}{\partial\hat{x}^4}+\frac{\partial^2\hat{w}}{\partial\hat{t}^2}+\hat{c}\frac{\partial\hat{w}}{\partial\hat{t}}-[\hat{N}+\alpha_1\Gamma(\hat{w},\hat{w})]\frac{\partial^2\hat{w}}{\partial\hat{x}^2} = \alpha_2\sum_i^P\hat{V}_i^2(\hat{t})\left[\frac{1}{(1-\hat{w})^2}-\frac{1}{(1+\hat{w})^2}\right] \times [H(\hat{x}-\hat{a}_i)-H(\hat{x}-\hat{b}_i)], \tag{10}$$

Table 1. Operator and parameter definitions corresponding to the equation of motion presented in equation (10).

$\Gamma(f_1(\hat{x},\hat{t}), f_2(\hat{x},\hat{t})) = \int_0^1 \frac{\partial f_1}{\partial \hat{x}} \frac{\partial f_2}{\partial \hat{x}}\, \mathrm{d}\hat{x}$
$\hat{c} = \frac{cl^4}{EIT}$
$\hat{N} = \frac{Nl^2}{EI}$
$\hat{a}_i = \frac{a_i}{l}$
$\hat{b}_i = \frac{b_i}{l}$
$\alpha_1 = 6\left(\frac{d}{h}\right)^2$
$\alpha_2 = \frac{6\varepsilon_0 l^4 {V_C}^2}{Eh^3 d^3}$

with operators and parameters defined as shown in table 1 and with boundary conditions given by

$$\hat{w}(0,\hat{t}) = 0, \qquad \hat{w}(1,\hat{t}) = 0,$$
$$\left.\frac{\partial \hat{w}}{\partial \hat{x}}\right|_{(0,\hat{t})} = 0, \qquad \left.\frac{\partial \hat{w}}{\partial \hat{x}}\right|_{(1,\hat{t})} = 0. \tag{11}$$

As the form of the forcing presented in equation (10) is difficult to analyse directly, it proves convenient to approximate the spatially-dependent portion of the forcing, through a truncated Taylor series expansion, according to

$$\left[\frac{1}{(1-\hat{w})^2} - \frac{1}{(1+\hat{w})^2}\right] \cong 4\hat{w} + 8\hat{w}^3, \tag{12}$$

which is valid for 'small' $\hat{w}$. This results in a new approximative equation of motion of the form

$$\frac{\partial^4 \hat{w}}{\partial \hat{x}^4} + \frac{\partial^2 \hat{w}}{\partial \hat{t}^2} + \hat{c}\frac{\partial \hat{w}}{\partial \hat{t}} - [\hat{N} + \alpha_1 \Gamma(\hat{w},\hat{w})]\frac{\partial^2 \hat{w}}{\partial \hat{x}^2} = \alpha_2 \sum_i^P \hat{V}_i^2(\hat{t})(4\hat{w} + 8\hat{w}^3)[H(\hat{x} - \hat{a}_i) - H(\hat{x} - \hat{b}_i)]. \tag{13}$$

Note that in contrast to a single electrode system, only odd-powered electrostatic terms appear in this equation of motion. In addition, it should be noted that the Taylor series approximation proves fairly accurate even in the presence of very small geometric asymmetries (e.g., those on the order of manufacturing tolerances), which could give rise to even-powered terms and, in turn, small direct excitation and quadratic nonlinear parametric effects (see section 5 for additional details).

As the electrodes shown in figure 1 are capable of providing ac or dc excitation (or perhaps both in an obvious extension not considered directly in this work), it proves convenient to separate the appropriate electrostatic terms. This results in a modified equation of motion of the form

$$\frac{\partial^4 \hat{w}}{\partial \hat{x}^4} + \frac{\partial^2 \hat{w}}{\partial \hat{t}^2} + \hat{c}\frac{\partial \hat{w}}{\partial \hat{t}} - [\hat{N} + \alpha_1 \Gamma(\hat{w},\hat{w})]\frac{\partial^2 \hat{w}}{\partial \hat{x}^2} = \alpha_2 \sum_m^Q \hat{V}_m^2(4\hat{w} + 8\hat{w}^3)[H(\hat{x} - \hat{a}_m) - H(\hat{x} - \hat{b}_m)] + \alpha_2 \sum_n^R \hat{\mathcal{V}}_n^2(\hat{t})(4\hat{w} + 8\hat{w}^3)[H(\hat{x} - \hat{a}_n) - H(\hat{x} - \hat{b}_n)], \tag{14}$$

where terms of the form $\hat{V}_m^2$ represent those due to dc actuation and those of the form $\hat{\mathcal{V}}_n^2(\hat{t})$ capture ac actuation. From this continuous system model a lumped-mass model is easily formulated.

3. Formulation of the lumped-mass model

Though the system model shown in equation (14) proves sufficient for some analysis, a lumped-mass model approach greatly facilitates investigation of the system's pull-in behavior and nonlinear response. Accordingly, the system's spatially-dependent dynamic variable, as present in equation (14), is decomposed using the system's mode shapes, namely,

$$\hat{w}(\hat{x},\hat{t}) = \sum_i^\infty A_i(\hat{t})\phi_i(\hat{x}). \tag{15}$$

Unfortunately, this results in a set of coupled nonlinear ordinary differential equations, which, in turn, requires a relatively cumbersome analysis that is of limited applicability (due to the approximate nature of MEMS models, in general). As such, it proves convenient to develop the nonlinear lumped-mass equation of motion from a linear analog of the modal equation where the applied axial load is neglected ($\hat{N} = 0$)—a valid assumption given that realistic values of $\hat{N}$ (as given, for example, in [9]) yield minimal distortion in the $\hat{N} = 0$ linear mode shapes (especially the first, which is used extensively in this work). This results in linear mode shapes which can be deduced in closed form from the governing equation [14]

$$\phi_i^{iv} - \omega_i^2 \phi_i = 0. \tag{16}$$

Noting that the first mode should be the dominant mode of the system, the modal expansion presented in equation (15) is approximated by a single term. Substituting the resulting mode (normalized through the inner product operator) in equation (14) and projecting back on the first mode (through the inner product operator) yields a final lumped-mass model of the form

$$\ddot{A} + \hat{c}\dot{A} + \left[\int_0^1 \phi^{iv}\phi\, \mathrm{d}\hat{x} - \hat{N}\int_0^1 \phi''\phi\, \mathrm{d}\hat{x}\right] A + \left[-4\alpha_2 \sum_m^Q \hat{V}_m^2 \int_{\hat{a}_m}^{\hat{b}_m} \phi^2\, \mathrm{d}\hat{x} - 4\alpha_2 \sum_n^R \hat{\mathcal{V}}_n^2(\hat{t}) \int_{\hat{a}_n}^{\hat{b}_n} \phi^2\, \mathrm{d}\hat{x}\right] A + \left[-\alpha_1 \Gamma(\phi,\phi)\int_0^1 \phi''\phi\, \mathrm{d}\hat{x}\right] A^3 + \left[-8\alpha_2 \sum_m^Q \hat{V}_m^2 \int_{\hat{a}_m}^{\hat{b}_m} \phi^4\, \mathrm{d}\hat{x} - 8\alpha_2 \sum_n^R \hat{\mathcal{V}}_n^2(\hat{t}) \int_{\hat{a}_n}^{\hat{b}_n} \phi^4\, \mathrm{d}\hat{x}\right] A^3 = 0, \tag{17}$$

where

$$(\dot{\bullet}) = \frac{\mathrm{d}(\bullet)}{\mathrm{d}\hat{t}}, \tag{18}$$

and

$$(\bullet)' = \frac{\mathrm{d}(\bullet)}{\mathrm{d}\hat{x}}. \tag{19}$$

To ensure harmonic excitation, the driving voltage, $\hat{\mathcal{V}}_n(\hat{t})$, is taken to be

$$\hat{\mathcal{V}}_n(\hat{t}) = \hat{\mathcal{V}}_n\sqrt{1 + \cos\hat{\omega}\hat{t}} = \hat{\mathcal{V}}_n\sqrt{1 + \cos\omega t} \tag{20}$$

Table 2. Operator and parameter definitions corresponding to the equation of motion presented in equation (21). Note that the prime operator has been redefined.

$z = A$
$\omega_0^2 = \int_0^1 \phi^{iv}\phi \,\mathrm{d}\hat{x} - \hat{N}\int_0^1 \phi''\phi \,\mathrm{d}\hat{x}$
$(\bullet)' = \dfrac{\mathrm{d}(\bullet)}{\mathrm{d}\tau}$
$\tau = \omega_0 \hat{t}$
$\Omega = \dfrac{\hat{\omega}}{\omega_0}$
$2\varepsilon\zeta = \dfrac{\hat{c}}{\omega_0}$
$\varepsilon\nu_1 = \dfrac{-4\alpha_2 \sum_m^Q \hat{V}_m^2 \int_{\hat{a}_m}^{\hat{b}_m} \phi^2 \,\mathrm{d}\hat{x} - 4\alpha_2 \sum_n^R \hat{V}_n^2 \int_{\hat{a}_n}^{\hat{b}_n} \phi^2 \,\mathrm{d}\hat{x}}{\int_0^1 \phi^{iv}\phi \,\mathrm{d}\hat{x} - \hat{N}\int_0^1 \phi''\phi \,\mathrm{d}\hat{x}}$
$\varepsilon\lambda_1 = \dfrac{-4\alpha_2 \sum_n^R \hat{V}_n^2 \int_{\hat{a}_n}^{\hat{b}_n} \phi^2 \,\mathrm{d}\hat{x}}{\int_0^1 \phi^{iv}\phi \,\mathrm{d}\hat{x} - \hat{N}\int_0^1 \phi''\phi \,\mathrm{d}\hat{x}}$
$\varepsilon(\chi + \nu_3) = \dfrac{-\alpha_1 \Gamma(\phi,\phi)\int_0^1 \phi''\phi \,\mathrm{d}\hat{x} - 8\alpha_2 \sum_m^Q \hat{V}_m^2 \int_{\hat{a}_m}^{\hat{b}_m} \phi^4 \,\mathrm{d}\hat{x} - 8\alpha_2 \sum_n^R \hat{V}_n^2 \int_{\hat{a}_n}^{\hat{b}_n} \phi^4 \,\mathrm{d}\hat{x}}{\int_0^1 \phi^{iv}\phi \,\mathrm{d}\hat{x} - \hat{N}\int_0^1 \phi''\phi \,\mathrm{d}\hat{x}}$
$\varepsilon\lambda_3 = \dfrac{-8\alpha_2 \sum_n^R \hat{V}_n^2 \int_{\hat{a}_n}^{\hat{b}_n} \phi^4 \,\mathrm{d}\hat{x}}{\int_0^1 \phi^{iv}\phi \,\mathrm{d}\hat{x} - \hat{N}\int_0^1 \phi''\phi \,\mathrm{d}\hat{x}}$

wherever applicable [15]. Following this substitution, equation (17) is rescaled to account for small damping and small electrostatic excitation (assumptions that are typically valid for MEMS resonators, especially those with high-Q). In addition, the sum of the nonlinear mechanical stiffness, which is generally hardening, and the nonlinear electrostatic stiffness, which is generally softening, is considered small, for reasons explained in section 5, and a nondimensional scaling parameter, ε, is introduced to facilitate analysis. This results in a final lumped-mass model of the form

$$z'' + 2\varepsilon\zeta z' + (1 + \varepsilon\nu_1 + \varepsilon\lambda_1 \cos\Omega\tau)z + \varepsilon(\chi + \nu_3 + \lambda_3 \cos\Omega\tau)z^3 = 0 \tag{21}$$

with parameters defined as in table 2. Interestingly enough, this lumped-mass model is nearly identical to that previously considered by the authors in the analysis of microelectromechanical (MEM) oscillators driven by non-interdigitated comb drives [10, 16]. Accordingly, the results of previous works on this subject are exploited throughout this work, especially in section 5 where the microbeam's dynamic response is considered.

Though the lumped-mass model developed above is likely sufficient for most analyses, an alternative model based on a least-squares curve fit of the electrostatic force may prove more desirable in studies where the accuracy of the truncated Taylor series approximation is insufficient or in studies where the operating regime for a given device (in terms of displacement) is well known. As their name implies, these alternative models can be developed by fitting the spatially-dependent portion of the exact electrostatic force (in this case after modal truncation and projection) to a cubic function of displacement over a specified displacement operating regime, while enforcing a specified linear force constraint (as realized by manipulating coefficients contained in ν_1, λ_1, ν_3 and λ_3). The net result of such an approach, as detailed in figure 2, is an improvement in the approximate force model over the specified range.

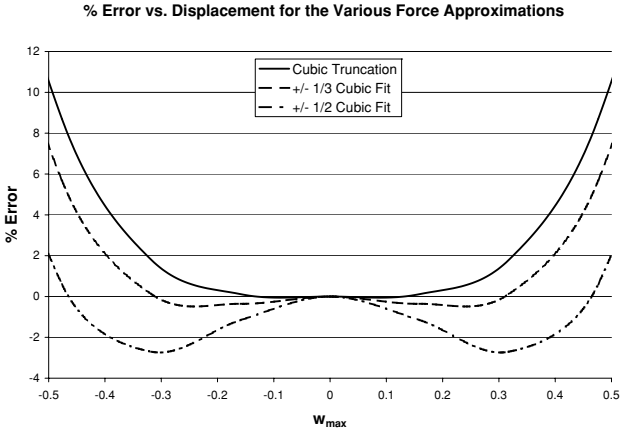

Figure 2. Force inaccuracy considered in terms of displacement (limited range) for the various approximative force models. Note that as expected, the models produced by curve fitting over a specified domain exhibit the least error over the given domain.

For example, the least-squares model fit over a displacement domain bounded by plus or minus one-half of the gap width, yields a maximum error of about 2.5%, approximately one-fourth of that produced by the truncated Taylor series model. Though such a difference may have minimal consequence with regard to introductory studies, similar to that presented here, future studies may benefit from the improvement in accuracy produced by such an approach, especially in cases where global dynamic phenomena (e.g., dynamic pull-in) are of principal concern.

Before proceeding with a discussion of the microbeam system's dynamic response, it proves prudent to briefly detail the operating range where the system model and attendant analysis (forthcoming) are believed to be sufficiently accurate for predictive design and conversely where limitations in the model and analysis constrain their applicability. To facilitate

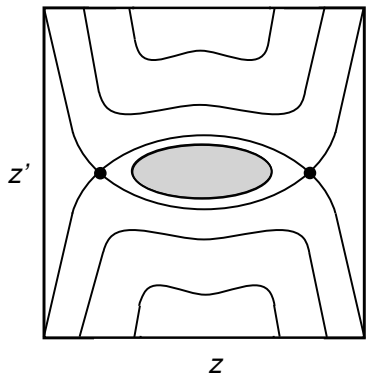

Figure 3. A qualitative phase plane for the proposed microbeam system. Note that only the *effective* dc electrostatic term (incorporating both dc voltage and some ac voltage effects) is included; inclusion of the ac term would yield perturbations in the solution trajectories shown. Also note the system model and attendant response analysis, as limited by force truncation and perturbation methods, respectively, are believed to be valid only in a local operating region akin to that shaded here.

this discussion, a qualitative phase plane, which captures the global behavior of the system, is included in figure 3. Note that the *effective* dc contribution due to both dc ($\hat{V}_m$) and ac ($\hat{\mathcal{V}}_n$) voltage effects has been included within the plot, but ac ($\hat{\mathcal{V}}_n$) voltage effects which directly lead to an *effective* ac contribution (and, in turn, to a distortion of the included solution trajectories) have been omitted. In other words, effects due to the term designated ν_1 (which depends on both $\hat{V}_m$ and $\hat{\mathcal{V}}_n$) have been included, while those effects due to λ_1 (which depends on only $\hat{\mathcal{V}}_n$) have been neglected.

Constraints relating to the system model can be generally attributed to the truncation of the Taylor series expansion of the electrostatic force model. Since this truncation requires a magnitude constraint on $\hat{w}$ the system model is believed to be accurate only for a limited range of z. Accordingly, the model should only be applied to the predictive design of devices operating in a displacement range bounded by a conservative fraction of the system's gap width, an operating range that is similar to that of most electrostatic sensors and actuators. Constraints relating to the included analysis, discussed in more detail throughout the work, can be generally attributed to the nature of the perturbation technique employed. In particular, the local averaging technique employed in section 5 is applicable only to the local dynamics contained within the heteroclinic cycle (connecting the two saddle points) depicted in figure 3. The analysis of system responses near or outside of this orbit, and thus the analysis of phenomena like dynamic pull-in, would be better facilitated by more global techniques such as those presented in previous works, including [17, 18]. In light of the limitations detailed above, a conservative qualitative operating region, completely enclosed by the heteroclinic cycle and bounded by a conservative fraction of the system's gap width, has been highlighted in figure 3. Within this region, the model and analysis included here should be sufficiently accurate to allow for the predictive design of the proposed devices operated near resonance.

Table 3. Parameter values for a representative microbeam system.

$E = 158$ GPa
$\rho = 2300$ kg m^{-3}
$l = 150$ μm
$h = 1$ μm
$b = 10$ μm
$d = 1$ μm
$N = 100$ μN

4. Pull-in

Though the impetus of the present study was to explore the nonlinear behavior of a parametrically-excited microbeam system, as with any electrostatically-actuated MEMS device, it is imperative that the system's pull-in behavior be considered as well. Accordingly, the static pull-in behavior of the system is considered in this section and the dynamic pull-in behavior is discussed, albeit briefly, in the forthcoming section, following a discussion of the system's nonlinear response.

Perhaps the most common 'failure mode' considered in the design of resonant MEMS devices is static pull-in (see, for example, [8, 19–22]). That is, the operating condition (or conditions in the case of multiple inputs) that leads to destabilization of the system's static operating point. This failure in the proposed parametrically-excited microbeam system is caused by the presence of an electrostatic load in excess of the system's static load bearing capacity. Analytically, this equates to the presence of a negative net linear stiffness in the system's equation of motion. Alternatively, from a bifurcation point of view, the point at which the failure occurs corresponds to a pitchfork bifurcation in which the stable central equilibrium is destabilized through a merging with the symmetric pair of unstable equilibria. For the system in question here, it is easily shown that the criterion for pull-in is given by

$$\int_0^1 \phi^{iv}\phi \,\mathrm{d}\hat{x} - \hat{N}\int_0^1 \phi''\phi \,\mathrm{d}\hat{x} - 4\alpha_2 \sum_m^Q \hat{V}_m^2 \int_{\hat{a}_m}^{\hat{b}_m} \phi^2 \,\mathrm{d}\hat{x} - 4\alpha_2 \sum_n^R \hat{\mathcal{V}}_n^2 \int_{\hat{a}_n}^{\hat{b}_n} \phi^2 \,\mathrm{d}\hat{x} = 0, \tag{22}$$

which, in contrast to most MEM devices, is dependent on both the dc and ac actuation voltages, an effect which can be directly attributed to the form of the excitation used to generate a purely-harmonic excitation.

To explore the static pull-in behavior of the proposed system in further detail, consider a system featuring parameters consistent with those presented in table 3 with a single electrode pair (actuated by a single dc voltage input) spanning the beam's length. This system is governed by a static equation of the form

$$\left[\int_0^1 \phi^{iv}\phi \,\mathrm{d}\hat{x} - \hat{N}\int_0^1 \phi''\phi \,\mathrm{d}\hat{x} - 4\alpha_2\hat{V}_0^2\int_0^1 \phi^2 \,\mathrm{d}\hat{x}\right] A + \left[-\alpha_1\Gamma(\phi,\phi)\int_0^1 \phi''\phi \,\mathrm{d}\hat{x} - 8\alpha_2\hat{V}_0^2\int_0^1 \phi^4 \,\mathrm{d}\hat{x}\right] A^3 = 0. \tag{23}$$

Evoking the fact that pull-in should occur when the net linear stiffness becomes negative, it can be shown that the system

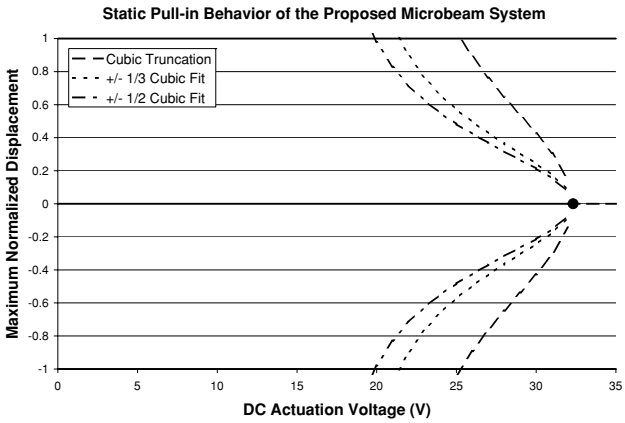

Figure 4. Static deflection behavior of the proposed microbeam system as predicted via cubic truncation of the forcing and via curve fitting.

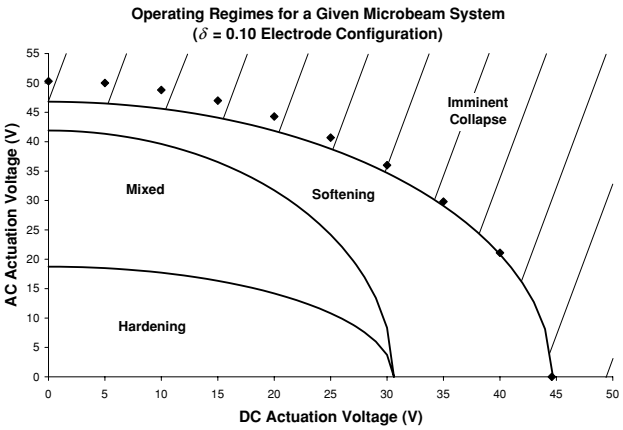

Figure 5. A representative two-parameter 'pseudo-static' pull-in chart. Note that collapse is predicted to occur beyond the noted boundary in the two-parameter input voltage space and that the diamonds correspond to points of predicted 'pseudo-static' pull-in, as obtained via simulation. Also note that collapse is possible below the boundary as dictated by the nature of the system's nonlinear response and input frequency.

should exhibit pull-in at approximately 32.3 V. As shown in figure 4, this prediction is entirely compatible with the behavior governed by equation (23). In fact, due to the enforcement of a linear force constraint in the previously proposed curve fitting techniques, the predicted static pull-in voltage is identical in all three system models developed in the present work (as evident from figure 4).

While the preceding example details the pull-in behavior of a single electrode pair system actuated via a dc voltage, a more relevant example for present purposes is a microbeam system with multiple electrostatic actuation voltages (ac and dc). An interesting feature of this system is that due to the form of excitation, namely its dependence on the square of the input voltage(s) (and the presence of both ac and dc voltage terms in the system's net linear stiffness term), its effective 'pseudo-static' pull-in (the term is used informally here to designate the operating condition(s) that results in a loss of stability for the trivial solution) behavior depends on both the system's ac and dc actuation voltages. Accordingly, pull-in is not governed by a point in a single input parameter space, but rather a curve in a two-parameter input space that depends on the electrode geometry of the proposed system. To examine this further consider a three-electrode pair system (similar to that depicted in figure 1), which exhibits a newly defined electrode characteristic $\delta = 0.10$, where δ is defined as half the nondimensional length of the center (ac) electrode. Again, noting that pull-in will occur when the effective linear stiffness becomes negative, the two-parameter 'pseudo-static' pull-in curve depicted in figure 5 can be developed. As figure 5 indicates, 'pseudo-static' pull-in is expected for all voltage input combinations that exceed the predicted threshold. To confirm the validity of this, the system governed by equation (21) was simulated and the respective pull-in points, depicted in figure 5, were determined. As evident from the figure, the predicted pull-in conforms quite well with the simulated results and while there is some discrepancy for larger ac voltages, this can likely be attributed to dynamic effects. It should be noted that while pull-in is predicted for *all* operating conditions beyond the curve presented, collapse is possible for operating conditions below the curve as well, as dictated by the nature of the nonlinear response and the ac voltage input's frequency (as described in section 5).

5. Dynamic response

With the static pull-in behavior largely characterized, attention can turn towards the focus of the present work: the microbeam system's dynamic response, the nature of which is perhaps best characterized through the equation of motion presented in equation (21). As noted in section 3, this model is identical in form to that considered by the authors in previous works, but with different system parameters [10, 16]. Accordingly, interested readers are directed to [16] for detailed information beyond that presented here (including a detailed analysis of the various nonlinear solutions' existence and stability).

As noted in section 3, the equation of motion presented in equation (21) is based on the assumption of 'small' excitation and damping, which is typically valid in MEMS resonators. It is also noted that the sum of the hardening nonlinearity, due to mechanical stiffness effects, and the softening nonlinearity, due to electrostatic stiffness effects, is also assumed to be small (as achieved through manipulation of the dc bias voltage); this assumption is put in place to distinguish the response of the proposed system with that of electrostatic devices dominated by nonlinear mechanical effects. Systems of this type exhibit a nonlinear response that is largely unaffected by electrostatic nonlinearities and thus their response is generally compatible with mechanically-hardening nonlinear oscillators with linear parametric excitation, a topic which has been extensively covered in nonlinear vibrations literature and thus is not considered here (see, for example, [23]).

To analyse the equation of motion presented in equation (21) it proves convenient to invoke perturbation techniques, which work well with the assumptions detailed above. In addition, damping is assumed to be zero ($\zeta = 0$) as it has a minimal effect on the qualitative nature of the nonlinear response (note that the effects of small damping are discussed in some detail in [16]). To facilitate the perturbation approach, in this case the method of averaging, a standard constrained

coordinate transformation is introduced, as given by

$$z(\tau) = a(\tau)\cos\left(\frac{\Omega\tau}{2} + \psi(\tau)\right), \tag{24}$$

$$z'(\tau) = -a(\tau)\frac{\Omega}{2}\sin\left(\frac{\Omega\tau}{2} + \psi(\tau)\right). \tag{25}$$

In addition, since near-resonant behavior is the principal operating regime of the proposed system, a detuning parameter, σ is introduced, as given by

$$\Omega = 2 + \varepsilon\sigma. \tag{26}$$

Separating the resulting equations and averaging them over the period $4\pi/\Omega$ in the τ-domain results in the system's averaged equations, in terms of amplitude and phase, which are given by [10, 16]

$$a' = \tfrac{1}{8}a\varepsilon[-8\zeta + (2\lambda_1 + a^2\lambda_3)\sin 2\psi] + \mathcal{O}(\varepsilon^2), \tag{27}$$

$$\psi' = \tfrac{1}{8}\varepsilon[3a^2(\chi + \nu_3) + 4\nu_1 - 4\sigma + 2(\lambda_1 + a^2\lambda_3)\cos 2\psi] + \mathcal{O}(\varepsilon^2). \tag{28}$$

The steady-state behavior of the proposed system is then determined by considering the time-invariant dynamics of the averaged equations presented in equations (27) and (28), as recovered by setting $(a', \psi') = (0, 0)$. This process yields a trivial solution and three nontrivial solution branches, the first two of which have amplitudes and phases (note that phases shifted by a multiple of π equate to the same physical response) given by [10, 16]

$$a_1 = \pm\sqrt{\frac{4\sigma + 2\lambda_1 - 4\nu_1}{3(\chi + \nu_3) - 2\lambda_3}}, \tag{29}$$

$$\psi_1 = \frac{\pi}{2}, \tag{30}$$

and

$$a_2 = \pm\sqrt{\frac{4\sigma - 2\lambda_1 - 4\nu_1}{3(\chi + \nu_3) + 2\lambda_3}}, \tag{31}$$

$$\psi_2 = 0. \tag{32}$$

Generally speaking, these two sets of solution branches are very similar to those typically seen in a simple nonlinear oscillator, in that the sign of the term under the square root sign dictates their existence with respect to forcing frequency (detuning). However, their relationship to the system's overall nonlinear characteristic, is somewhat unique. In particular, due to the differing denominators of each response branch, a single effective nonlinearity, which captures the system's nonlinear behavior cannot be obtained. Rather multiple effective nonlinearities are required, which reveal the system's nonlinear nature only when collectively considered [10, 16]. To verify this, two effective nonlinearities are defined, as taken from the denominators of a_1 and a_2, according to

$$\eta_1 = 3(\chi + \nu_3) - 2\lambda_3 \tag{33}$$

and

$$\eta_2 = 3(\chi + \nu_3) + 2\lambda_3. \tag{34}$$

As brief analysis will reveal, the nature of the system's frequency response differs with the signs of η_1 and η_2. In particular, for $\eta_1 > 0$ and $\eta_2 > 0$ the system locally exhibits a hardening nonlinearity, for $\eta_1 < 0$ and $\eta_2 < 0$ a softening nonlinearity, and for $\eta_1 > 0$ and $\eta_2 < 0$ and $\eta_1 < 0$ and $\eta_2 > 0$ mixed nonlinearities wherein the response branches bend toward or away from one another near resonance [10, 16]. To summarize this result the nonlinear nature of the response can be characterized through consideration of the $\gamma_3 - \lambda_3$ parameter space as shown in figure 6, where γ_3, the effective nonlinear stiffness coefficient, is defined according to

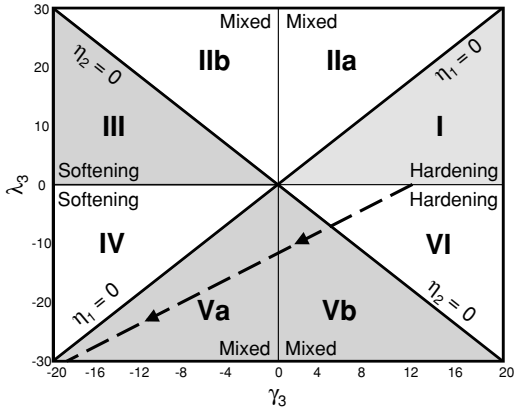

Figure 6. The γ_3–λ_3 parameter space (From [16]). Those regions designated I and VI exhibit hardening (or quasi-hardening) nonlinear characteristics, those designated III and IV exhibit softening (or quasi-softening) nonlinear characteristics, and those designated IIa, IIb, Va and Vb exhibit mixed nonlinear characteristics. The devices in question are expected to operate only in the regions designate IV, Va, Vb and VI. Note that the line included on the plot represents the trajectory followed by the proposed system under a fixed dc voltage of 5 V and a fluctuating ac voltage.

$$\gamma_3 = \chi + \nu_3, \tag{35}$$

and λ_3 is the nonlinear parametric excitation amplitude.

While the signs of η_1 and η_2 largely dictate the nature of the system's nonlinear frequency response, the third solution branch, with amplitude given by [10, 16]

$$a_3 = \pm\sqrt{\frac{-2\lambda_1}{\lambda_3}}, \tag{36}$$

can play a significant role as well. However, since the third solution branch's existence is dependent on the sign of λ_1/λ_3, a term that will be positive for most viable configurations of the present system, these solutions are largely unobtainable and thus only three topologically distinct frequency responses are obtainable here, namely, responses which exhibit hardening, softening, or mixed (response branches bending away from one another) nonlinear characteristics (corresponding to regions IV–VI in figure 6).

To explore the proposed system's nonlinear response further, consider again the three-electrode pair system that was introduced in the preceding section. According to the aforementioned results, the proposed system should be able to exhibit one of three possible frequency response types depending on where in the nonlinear parameter space (or in the corresponding two-parameter input voltage space, as shown in figure 5) the system lies. This is confirmed by figures 7–9, which show the system's nonlinear response at three distinct operating conditions in the parameter space shown in figure 5. As predicted, figure 7 depicts a classical

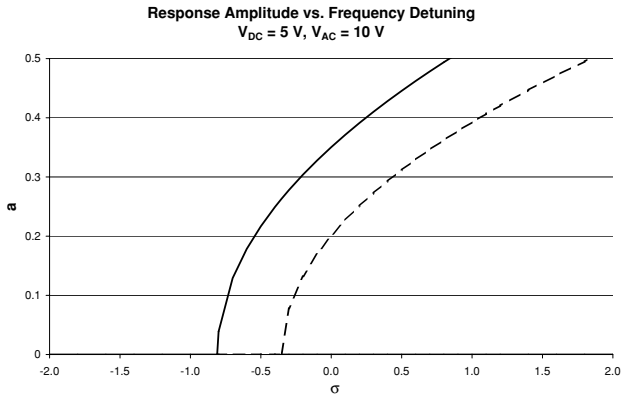

Figure 7. Analytically produced frequency response for a representative oscillator excited with 5 V dc and 10 V ac. Note the hardening nonlinear characteristic. Also note that here and in figures 8 and 9 solid lines indicate a stable response and dashed lines an unstable response.

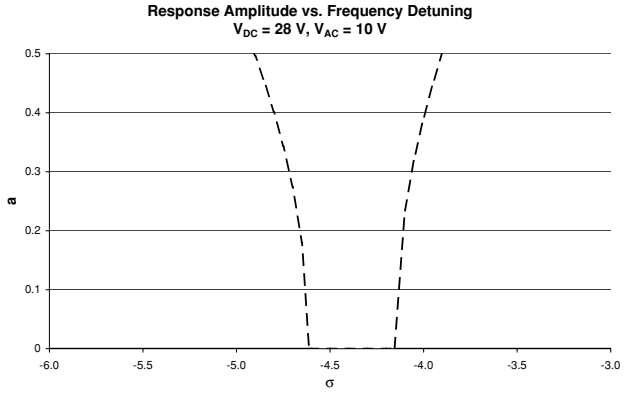

Figure 8. Analytically produced frequency response for a representative oscillator excited with 28 V dc and 10 V ac. Note the mixed nonlinear characteristic.

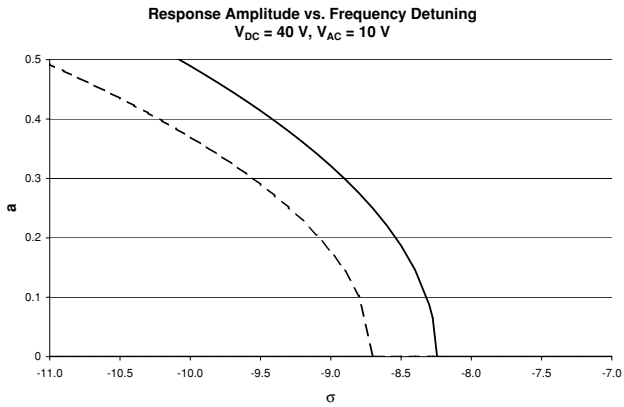

Figure 9. Analytically produced frequency response for a representative oscillator excited with 40 V dc and 10 V ac. Note the softening nonlinear characteristic.

hardening frequency response, figure 9 a classical softening frequency response, and perhaps more interestingly, figure 8 a frequency response wherein the nontrivial response branches bend away from one another near resonance (though the latter of these responses may prove problematic in implementation, as certain input frequencies lead to unbounded responses—this may be reconcilable through the inclusion of higher-order nonlinearities). As evident from figures 7–8, each of these responses displays desirable characteristics. Perhaps most notably, they each exhibit a stable, non-resonant zero response, which in implementation corresponds to nearly ideal stopband rejection, and rapid response roll-off—highly desirable features for any resonant microbeam system.

While the results detailed above are a positive indication of the flexibility of the proposed microbeam system, especially with regard to the potential implementation of softening or hardening devices on the same geometrical platform, it is important to point out the study's limitations. First, while softening behavior is analytically predicted to exist for certain operating conditions, this operating regime exists close to the predicted 'pseudo-static' pull-in point. Accordingly, the system is operating in a regime where the *a priori* assumptions begin to break down, most notably due to the presence of $\mathcal{O}(1)$ electrostatic effects. As such, softening regimes may be quite difficult to realize in practical applications. While simulations may provide some clarification of this issue, those completed to date have not yielded definitive results (softening responses have been found for the system design presented here, but a wide variety of designs have not yet been considered), as such simple experimental studies will likely be needed to provide definitive evidence of the softening regime.

Another limitation of the results presented here is that they are based on an approximate force model. While this is well suited for characterizing local behavior, it does not accurately capture large-amplitude nonlinear frequency response behavior or global system failures, such as those associated with dynamic pull-in. Additionally, the system model does not account for force imbalances arising from either manufacturing imperfections or non-uniform residual stresses. To ensure proper operation, a numerical simulation of a lumped-mass analog of the system presented here was constructed in Simulink^{TM}. The simulation incorporated precise models of the system's linear elastic restoring force and electrostatic restoring and driving forces (no expansions or truncations were used) and an approximative model of the system's nonlinear elastic restoring force. Additionally, asymmetries in the force model arising from electrostatic or elastic imbalance were introduced, to ensure that they did not compromise operation. In general, the results proved quite promising. Though desirable response features, such as absolute stopband rejection, began to deteriorate in the presence of asymmetries, the hardening region proved to be quite robust, with amplitudes and bifurcation points remaining largely invariant (i.e., they shift both in frequency and amplitude by only a small per cent), even in the presence of fairly large asymmetries (up to 10% gap asymmetry or, in the case of elastic asymmetry, 10% static offset). The softening region proved significantly less robust, but even it featured little degradation in the presence of asymmetries on the order of a few per cent, which is about all that can be expected given the proximity of this operating condition to 'pseudo-static' pull-in.

6. Design considerations

As evident from the results of the preceding sections, the proposed microbeam system potentially offers great flexibility for future resonant sensor and filter designs. However, inherent to this flexibility are some design complications. In particular, unlike classical parametrically-excited MEM oscillators whose response can be manipulated via parameters which can be varied in a largely independent manner through the design of the comb drives, the behavior of the system in question is tied to a relatively small number of parameters which when altered affect both the linear and nonlinear response characteristics, and do so in a manner constrained by the physics of the driving electrodes. This section attempts to summarize these issues in a manner that may prove useful for the practical design of such devices.

Of utmost importance with any resonant MEMS device, be it a sensor or filter, is the location and width of the system's resonance. Since the proposed system is based on parametric resonance, this is analogous to the classical problem of positioning and orientating a parametrically-excited system's 'wedge of instability', or more specifically, locating and specifying the width of the unstable region of the system's trivial solution (see, for example, [23, 10, 16]). For the device in question, this is done by dictating two distinct quantities: the system's purely mechanical natural frequency, which is dependent on the geometry of the microbeam, as well as the axial load in the structure (which is dependent on the nature of the fabrication process amongst other things), and the system's linear electrostatic force, which is largely dependent on the geometric configuration of the electrodes and the magnitude of the system's input voltages. Noting this, it can be shown that for the undamped system the instability region is bounded by the critical frequency (detuning) values of

$$\sigma = \nu_1 \pm \frac{\lambda_1}{2}, \tag{37}$$

and centered about the frequency (detuning) value of

$$\sigma = \nu_1, \tag{38}$$

as outlined in [16]. As evident from table 2, these critical frequency values, and thus the center frequency as well, are largely dependent on the input voltages of the system in terms of both location and relative distance. This dependence is confirmed in figure 10, which depicts the system's wedge of instability, for two different dc voltages, in the V_{ac}-Ω parameter space. Similarly, it can be shown that the electrode configuration, as manipulated through the geometric parameter δ (a relative measure of the length of the ac electrode), plays a significant role. In particular, increasing δ produces results consistent with increasing the ac actuation voltage and decreasing the dc actuation voltage for a fixed-δ system.

As highlighted in the previous section, the characteristic form of the system's nonlinearity, and thus the device's mode of nonlinear operation, is dependent on the system's location in the nonlinear parameter space depicted in figure 6, which in turn is dependent on the nonlinear mechanical and electrostatic characteristics of the system in question. This is further verified by figure 11, which shows a rudimentary design chart for characterizing this nonlinear parameter effect in terms of

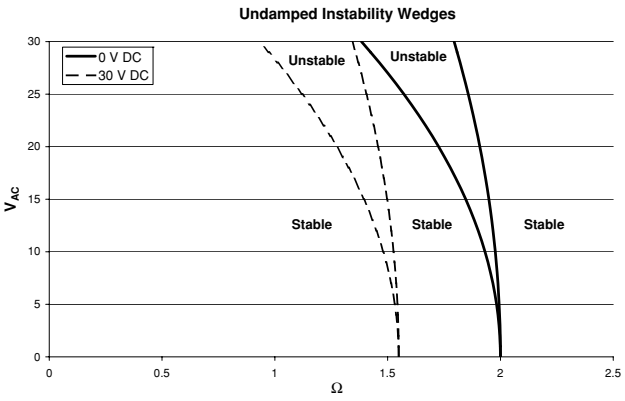

Figure 10. Linear instability wedges for the undamped microbeam system actuated at 0 V dc and 30 V dc, respectively. The system's zero response is unstable inside of the wedges and stable outside of the wedges. Note that as the dc voltage is increased the instability wedge shifts to the left in the parameter space.

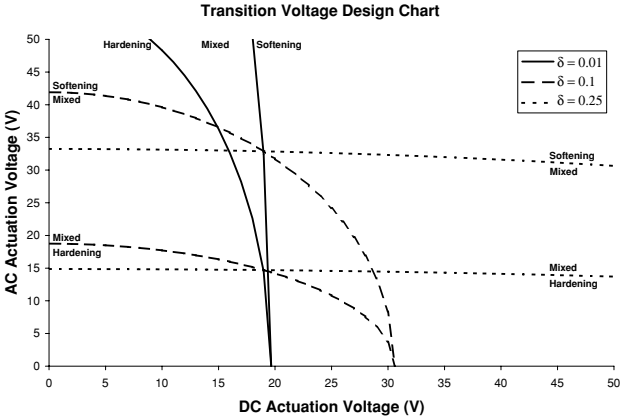

Figure 11. Sample design chart for predicting voltage transitions. Note that the 'lower' boundaries correspond to transitions between hardening and mixed nonlinear behavior and the 'upper' boundaries correspond to transitions between softening and mixed nonlinear behavior.

the input voltages and the design parameter δ. As expected, the relative size of the electrodes results in a relative weighting of the appropriate term in the force model, as previously seen in the course of linear design. Accordingly, it is clear that the nonlinear behavior of the proposed system and the location and width of its linear instability region are highly entwined.

In light of the dependent nature of the design of the microbeam system, the following iterative design strategy is proposed. To begin, the device's nonlinear mode of operation (most likely hardening, but potentially softening) and allowable operating voltage ranges should be specified. This, in turn, results in approximate magnitude constraints on the relative electrode size and nonlinear mechanical properties of the microbeam. These constraints, in conjunction with a specified purely mechanical natural frequency (or alternative geometric constraint), can then be used to generate a geometric design of the device in question. The width of the resulting instability zone can then be verified to ensure conformity with the desired characteristic and the system's 'pseudo-static' (and potentially dynamic) pull-in voltages can be computed to ensure proper device operation. System parameters can then

be iteratively 'tuned' until the system's behavior matches as closely as possible to the desired behavior, thereby yielding a resonant MEMS device with superior characteristics.

For reference purposes, it should be noted that the sample device presented in this work was developed via the design strategy detailed above. For this case, it was desirable to feature a device which exhibited hardening, softening and mixed nonlinear responses over a practical range of ac and dc voltages, in this case approximately 0–50 V. Noting this, viable ranges for δ, α_1 and α_2 were computed. Using these ranges, in conjunction with a nondimensional, purely-mechanical natural frequency target (somewhere on the order of 25, which corresponds to approximately 2.5 MHz) and realistic geometric constraints based on fabrication limitations (e.g. 1 μm minimum feature size), a potential beam geometry (i.e. l, b, t, d and δ) was produced (details of which can be found in table 3). Since a specific bandwidth was not needed and pull-in was found to occur outside of, or near the limits of, the voltage operating range, iteration was not needed. However, the beam configuration associated with *this* particular design problem did not appear to be over-constrained and thus bandwidth or pull-in correction via iterative 'tuning' would have been possible, as is generally believed to be the case.

7. Conclusion

As detailed throughout this work, parametrically-excited resonant microbeam systems and all of their attendant benefits, including an inherent flexibility, are realizable through the exploitation of a novel symmetric electrode configuration. Accordingly, it should be possible to exploit such designs for future use as resonant sensors or signal filters. Of course, the inherent flexibility which makes the proposed systems desirable comes with a cost, namely, inherent complexity (from a modeling and predictive design point of view). Whereas comb driven systems can be easily designed to exhibit a desired phenomenon (through manipulation of the comb drive structure), the proposed microbeam systems feature linear and nonlinear behavior that is somewhat entangled due to the reduced number of system parameters. Accordingly, future work will have to balance the reduction in size, reduced power consumption and geometric (manufacturing) simplicity of the proposed design with the design simplicity of its comb driven counterpart. Ongoing research is aimed at examining this trade-off and addressing a variety of unresolved issues, most notably obtaining experimental evidence of the softening response region and determining its viability as a robust operating point.

Acknowledgments

This work was graciously supported by the National Science Foundation under grant NSF-0428916. The authors would also like to thank Barry DeMartini and Jeff Moehlis for their contributions to this work.

References

[1] Napoli M, Baskaran R, Turner K and Bamieh B 2003 Understanding mechanical domain parametric resonance in microcantilevers *Proc. IEEE 16th Ann. Int. Conf. on Micro Electro Mechanical Systems (Kyoto, Japan)* pp 169–72

[2] Thundat T, Oden P I and Warmack R J 1997 Microcantilever sensors *Microscale Thermophys. Eng.* **1** 185–99

[3] Gui C, Legtenberg R, Tilmans H A C, Fluitman J H J and Elwenspoek M 1998 Nonlinearity and hysteresis of resonant strain gauges *J. Microelectromech. Syst.* **7** 122–7

[4] Abdel-Rahman E M, Younis M I and Nayfeh A H 2002 Characterization of the mechanical behavior of an electrically actuated microbeam *J. Micromech. Microeng.* **12** 759–66

[5] Legtenberg R and Tilmans H A C 1994 Electrostatically driven vacuum-encapsulated polysilicon resonators, part I: design and fabrication *Sensors Actuators* A **45** 57–66

[6] Lifshitz R and Cross M C 2003 Response of parametrically driven nonlinear coupled oscillators with application to micromechanical and nanomechanical resonator arrays *Phys. Rev.* B **67** 134302

[7] Napoli M, Bamieh B and Turner K 2004 A capacitive microcantilever: modelling, validation, and estimation using current measurements *J. Dyn. Syst. Meas. Control* **126** 319–26

[8] Younis M I, Abdel-Rahman E M and Nayfeh A 2003 A reduced-order model for electrically actuated microbeam-based MEMS *J. Microelectromech. Syst.* **12** 672–80

[9] Younis M I and Nayfeh A H 2003 A study of the nonlinear response of a resonant microbeam to an electric actuation *Nonlinear Dyn.* **31** 91–117

[10] Rhoads J F, Shaw S W, Turner K L and Baskaran R 2005 Tunable microelectromechanical filters that exploit parametric resonance *J. Vib. Acoust.* **127** 423–30

[11] Zhang W and Turner K L 2004 Noise analysis in parametric resonance based mass sensing *Proc. ASME Int. Mech. Eng. Congress and Exposition (Anaheim, CA)*

[12] Dowell E H 1966 Nonlinear oscillations of a fluttering plate *AIAA J.* **4** 1267–75

[13] Bolotin V V 1963 *Nonconservative Problems in the Theory of Elastic Stability* (Oxford: Pergamon)

[14] Meirovitch L 1997 *Principles and Techniques of Vibrations* (Upper Saddle River: Prentice Hall)

[15] Turner K L, Miller S A, Hartwell P G, MacDonald N C, Strogatz S H and Adams S G 1998 Five parametric resonances in a microelectromechanical system *Nature* **396** 149–52

[16] Rhoads J F, Shaw S W, Turner K L, Moehlis J, DeMartini B E and Zhang W 2006 Nonlinear parametric resonance in electrostatically-excited microelectromechanical systems *J. Sound Vib.* to be published

[17] Ashhab M, Salapaka M V, Dahleh M and Mezic I 1999 Melnikov-based dynamical analysis of microcantilevers in scanning probe microscopy *Nonlinear Dyn.* **20** 197–220

[18] Ashhab M, Salapaka M V, Dahleh M and Mezic I 1999 Dynamic analysis and control of microcantilevers *Automatica* **35** 1663–70

[19] Chowdhury S, Ahmadi M and Miller W C 2005 A closed-form model for the pull-in voltage of electrostatically actuated cantilever beams *J. Micromech. Microeng.* **15** 756–63

[20] Krylov S and Maimon R 2004 Pull-in dynamics of an elastic beam actuated by continuously distributed electrostatic force *J. Vib. Acoust.* **126** 332–42

[21] Pamidighantam S, Puers R, Baert K and Tilmans H A C 2002 Pull-in voltage analysis of electrostatically actuated beam structures with fixed-fixed and fixed-free end conditions *J. Micromech. Microeng.* **12** 458–64

[22] Krylov S, Harari I and Cohen Y 2005 Stabilization of electrostatically actuated microstructures using parametric excitation *J. Micromech. Microeng.* **15** 1188–204

[23] Nayfeh A H and Mook D T 1979 *Nonlinear Oscillations* (New York: Interscience (Wiley-Interscience))